Hydrogen storage in Pd clusters

2000 J. Phys.: Condens. Matter 12 6799

(http://iopscience.iop.org/0953-8984/12/30/310)

J. Phys.: Condens. Matter **12** (2000) 6799–6823. Printed in the UK PII: S0953-8984(00)10566-1

Hydrogen storage in Pd clusters

N Watari†, S Ohnishi‡ and Y Ishii§

† NEC Informatec Systems Limited, Miyazaki 4-1-1, Miyamae-ku, Kawasaki, Kanagawa 216-8555, Japan
‡ NEC Fundamental Research Laboratory, Miyukigaoka 34, Tsukuba, Ibaraki 305-8501, Japan
§ Department of Physics, Chuo University, Kasuga, Bunkyo-ku, Tokyo 112-8551, Japan

Received 4 January 2000, in final form 4 May 2000

Abstract. Hydrogen storage in a Pd cluster is studied theoretically using a self-consistent density-functional scheme with a norm-conserving pseudopotential. We mainly focus on the cuboctahedral $Pd_{13}H_n$ clusters with $n = 1$, 6, 8, and 14. Two stable sites for hydrogen adsorption are found; one is slightly inside the square face of the cluster and the other is outside of the triangular face. Electronic states relevant to hydrogen adsorption are well described by the cluster-centre electronic states (CCSs); this term refers to the states produced by the centre cluster (hydrogen atoms and the centre Pd atom) interacting with peripheral Pd atoms. When the hydrogen atoms are adsorbed inside the tetrahedral face, the cluster is stabilized by expanding the Pd–Pd distance by 3.7%, which is close to the lattice expansion in the β-phase of bulk PdH. As the face-centred-cubic bulk can be fully 'clusterized' by these clusters, we estimate the entropy change of the bulk upon transition as the change in configuration entropy between these clusters.

1. Introduction

The history of the study of Pd hydride dates back to Graham's work in 1866 [1]. Graham found that hydrogen is highly soluble in Pd metal: Pd can store hydrogen at 643 times its own volume at room temperature. There have been many studies on the Pd–H system [2–4] and its superconductivity [5–7]. It has been attracting much attention because of its increasing importance as a clean energy-conversion medium. Upon the absorption of hydrogen at room temperature up to a ratio x for PdH_x of 0.025–0.030, the lattice parameter of palladium metal slightly increases from 7.353 au to 7.358 au (0.07%). This low-concentration phase is called the α-phase. Above $x \approx 0.6$, the β-phase, in which a lattice parameter is expanded to 7.608 au (3.5%), is obtained as a single phase. At a stoichiometric concentration of $x = 1$, it is believed that all the octahedral sites (o-sites) are filled and an ideal NaCl structure is attained.

Both experimental and theoretical studies have been extensively carried out on hydrogen sites in Pd [8]. Theoretical analyses on hydrogen sites in Pd based on first-principles calculations were given by Ho *et al* [9], a series of works by Elsässer *et al* [10, 11], and Krimmel *et al* [12]. They pointed out the possibility of hydrogen occupation at the tetrahedral sites (t-sites) induced by lattice relaxation and distortion. Recent clustering model studies on vacancies focused only on the o-site hydrogen distribution in the α- and β-phases [13]. The mechanisms of the phase transition and the hydrogen siting in the β-phase, however, have not been elucidated yet.

Theoretical studies on the electronic structure of metal hydrides began with the band calculations by Switendick in 1970 [14]. The following features were obtained by band calculations [15–17] and a cluster model calculation [18]:

0953-8984/00/306799+25$30.00

(1) The Pd–H bonding band is constructed from Pd s, p, d states under the Pd d band.
(2) The Pd d band is lowered and the Fermi level is placed in the s–p band above the Pd d band.
(3) The density of states (DOS) at the Fermi level is exceedingly small but increases as the hydrogen concentration increases. These states at the Fermi level are thought to be the cause of the superconductivity.
(4) The density of states of H 1s is large above and below the Pd d band.

We have shown in previous papers [19, 22] that the stable atomic structure of Pt_{13} and Pd_{13} clusters is a cuboctahedron and that the electronic structure of Pt_{13} and hydrogen adsorbed on Pt_{13} clusters is essentially understood in the context of the electronic shell model. In this paper, we study the mechanism of the hydrogen storage in Pd by means of cluster models: cuboctahedral Pd_{13}/H_n with $n = 1, 6, 8$, and 14. Since the cluster model approach is convenient for use in studying the electronic structures in terms of the chemical bonding based on atomic orbitals of Pd and H, it allows us to investigate the stability of relevant clusters in the β-phase of PdH_x at $x > 0.6$ in the bulk. The present numerical calculation scheme is based on the linear combination of pseudo-atomic orbitals (LCPSAO) method using a norm-conserving pseudopotential and is fully described in our previous works [19, 20]. The generalized gradient approximation (GGA) exchange–correlation energy due to Perdew, Burke, and Ernzerhof (PBE) [21] is included self-consistently.

In section 2, the hydrogen storage mechanism of the Pd cluster is studied by using cluster model calculations for cuboctahedral Pd_{13}/H clusters. As discussed in section 3, the face-centred-cubic (fcc) lattice is decomposable into 13-atom-cuboctahedron clusters without absence or overlap of the atoms. We study the electronic structures of the bulk system and compare the results with those from the cluster model. In section 4, we discuss the hydrogen-bonding nature of 13-atom-cuboctahedral clusters compared with those of smaller clusters. We propose a structural model for the β-phase and estimate the configurational entropy change for the α–β transition. Finally we discuss the enhancement in hydrogen adsorption which depends on the number of hydrogen atoms.

2. Atomic and electronic structures of $Pd_{13}H_n$ clusters

2.1. Atomic structures

To investigate the stable site for the hydrogen positioning, we have calculated the total energies for Pd_{13} clusters and hydrogen atoms by changing the distance R_H between the cluster centre and the hydrogen atom(s). Figures 1(a) and 1(b) show the geometries of $Pd_{13}H_6$ and $Pd_{13}H_8$ clusters; the H atom is placed on a line connecting the cluster-centre atom and the square-face centre for $Pd_{13}H_6$ and the triangular-face centre for $Pd_{13}H_8$. Both $Pd_{13}H_6$ and the $Pd_{13}H_8$ clusters are of O_h symmetry. In a $Pd_{13}H_1$ cluster the H atom is placed on a line connecting the centre atom and the square-face centre. In this paper, hereafter, 'hydrogen adsorption to the triangular or square face' means adsorption somewhere on the line connecting the cluster-centre atom and the centre of the triangular or square face, respectively.

We define the total energy for an adsorbed H atom as the total energy of $Pd_{13}H_n$ minus those of a Pd_{13} cluster and hydrogen molecules divided by the number of hydrogen atoms. Here the Pd_{13} cluster has a total energy of -376.588 Hartree for the Pd–Pd distance $R_{Pd} = 5.1$ au and the hydrogen molecule has a total energy of -1.05358 Hartree for the H–H distance 1.346 au.

The total energies for an H adsorbed in $Pd_{13}H_n$ ($n = 1, 6, 8$) are plotted in figure 2(a) as functions of R_H. The vertical lines in figure 2(a) indicate the values of R_H coinciding with the square or triangular faces, respectively. We have also made calculations for two

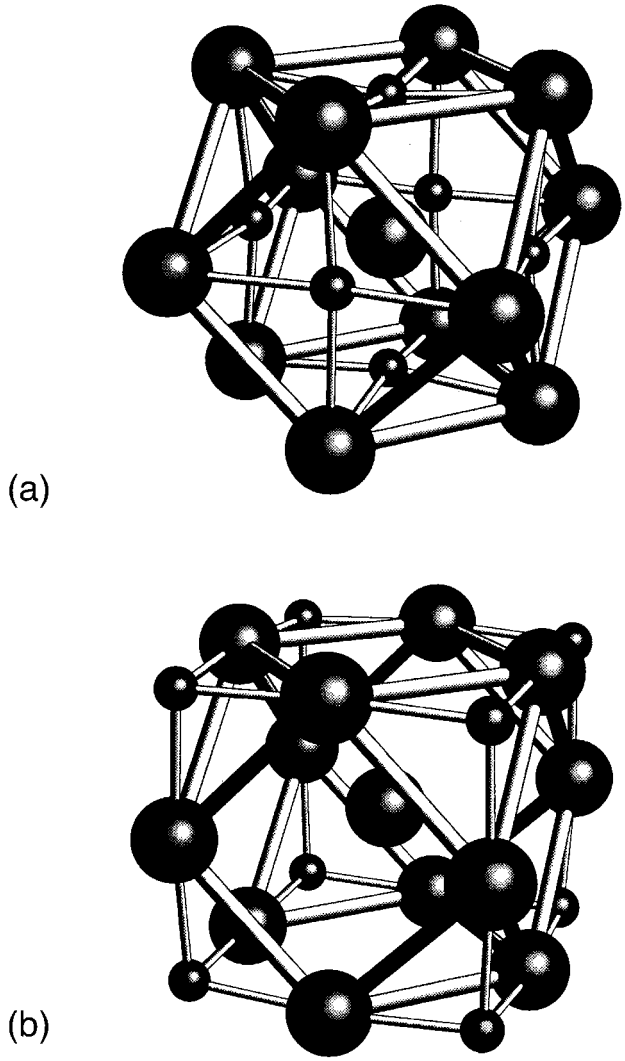

Figure 1. (a) The Pd_{13} cuboctahedron/H_6 cluster (site B′ adsorption). (b) The Pd_{13} cuboctahedron/H_8 cluster (site F adsorption).

different geometries. Figure 2(b) shows the total-energy curves for $Pd_{13}H_{6+2}$ (cuboctahedron) and $Pd_{13}H_8$ (icosahedron) clusters. In $Pd_{13}H_{6+2}$, six hydrogen atoms are fixed at positions slightly inside the square face, $R_H = 3.4$ au, and the two additional hydrogen atoms placed at centrosymmetric positions change their locations along the lines from the cluster centre through the triangular-face centres. In $Pd_{13}H_8$ (icosahedron), eight hydrogens are placed along the line connecting the centre atom and the triangular-face centre of an icosahedron to preserve the cubic symmetry. The plots for the icosahedron of $Pd_{13}H_8$ are obtained by changing the locations of H_8 along the lines connecting the centre atom and the triangular-face centre. We give a plot for $Pd_{13}H_8$ (cuboctahedron), which is the same as that in figure 2(a), for comparison. In the case of $Pd_{13}H_{6+2}$, it is remarkable that local minima in the total energies are located at similar values of R_H irrespective of the number of the hydrogens and the adsorption site.

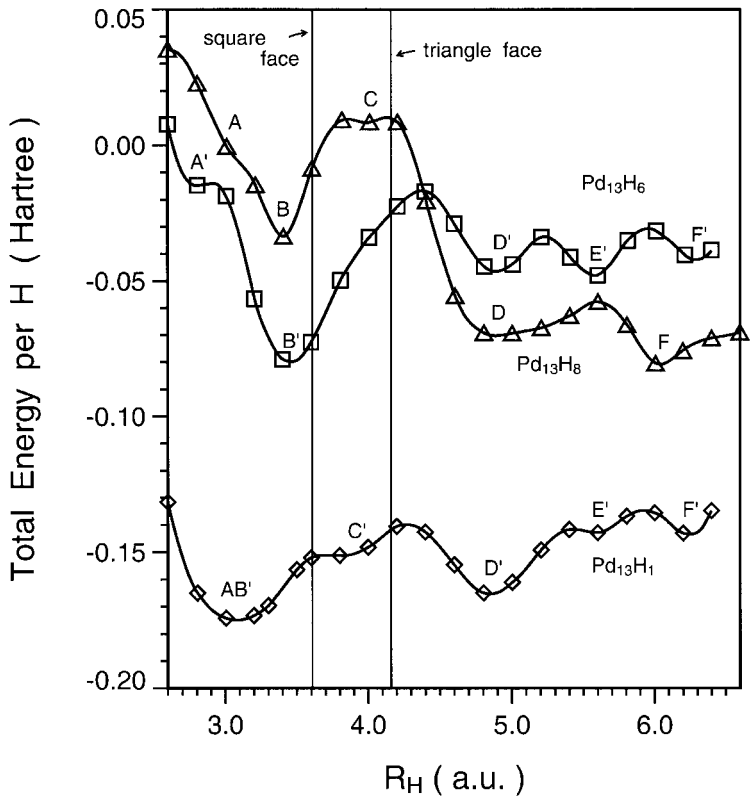

(a)

Figure 2. (a) Total energy per hydrogen atom for the Pd_{13} cuboctahedron/H_1 (◇), Pd_{13} cuboctahedron/H_6 (□), and Pd_{13} cuboctahedron/H_8 (△) clusters versus the distance of the hydrogen(s) from the cluster centre. The distance between Pd atoms R_{Pd} is fixed at 5.1 au. (b) The same for the Pd_{13} cuboctahedron/H_{6+2} (◇), Pd_{13} cuboctahedron/H_8 (△), and Pd_{13} icosahedron/H_8 (□) clusters.

The local minima are sequentially labelled A to F for the adsorptions to triangular faces of the cuboctahedron cluster, A′ to F′ for those to the square faces of the cuboctahedron cluster, and a to e for those to the triangular faces of the icosahedron cluster. The values of R_H (i) for inner sites B, B′, and b, (ii) for sites C, C′, and c, and (iii) for D, D′, and d seem to be independent of the face chosen and the symmetry of the Pd cluster, suggesting that these minima have nearly pseudo-spherical symmetry.

Various properties for $Pd_{13}H_6$ and $Pd_{13}H_8$ are listed in tables 1 and 2, respectively. Firstly, the total energies ΔE are calculated for a fixed value of R_{Pd} (=5.10 au), and the orbital populations of low-lying states and Mulliken charge are evaluated. The interatomic distance between H and the peripheral Pd, R_{H-Pd}, is calculated from R_{Pd} and R_H. After finding the optimal R_H, we relax the Pd–Pd distance R_{Pd} to minimize the total energy. A remarkable expansion in R_{Pd} is obtained for the C-site adsorption, where the total energy decreases to -0.064 Hartree per H atom, which is compatible with the most favourable B′-site adsorption. It is noteworthy that the B (or C) and B′ sites are close to the centre of a tetrahedron (t-site) and that of an octahedron (o-site), respectively, in an fcc crystal when cuboctahedral clusters are put together to make an fcc lattice as shown in section 3. The optimized distance between H and the peripheral Pd, R_{H-Pd}, is smaller than R_H (table 2). This value roughly corresponds

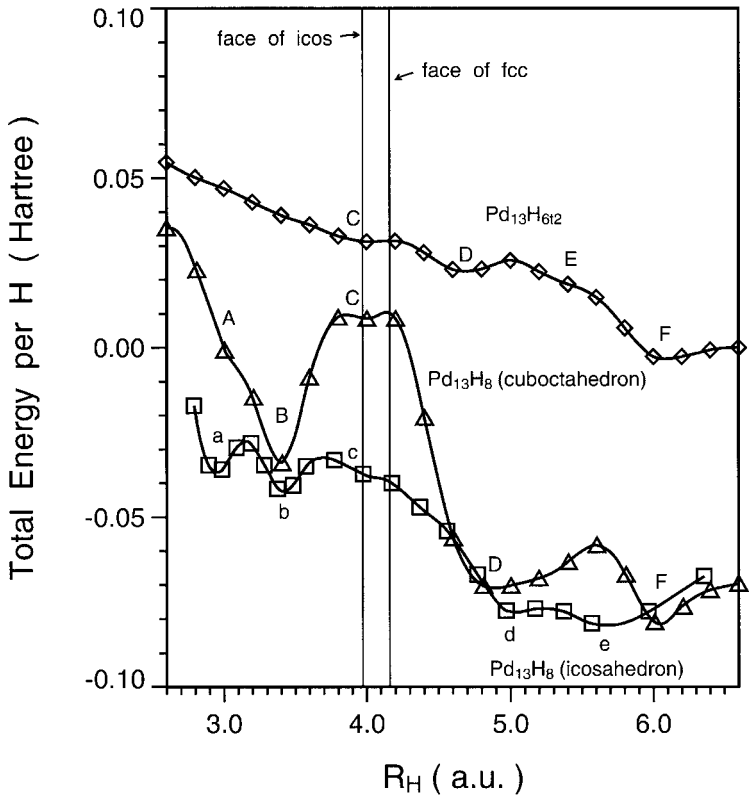

(b)

Figure 2. (Continued)

to the sum of the atomic radii for Pd and H. It should also be noted that the optimized Pd–Pd distance at the B site, 5.39 au, which is 3.7% longer than the experimental bulk Pd–Pd distance, 5.199 au [5], is very close to the experimental Pd–Pd distance of bulk PdH in the β-phase.

2.2. Electronic structures of clusters

Energy levels are shown as functions of R_H in figures 3(a), 3(b), and 3(c) for $Pd_{13}H_1$, $Pd_{13}H_6$, and $Pd_{13}H_8$, respectively, for a fixed $R_{Pd} = 5.1$ au. Here the levels are classified into three groups:

(1) the states above the Pd d levels, which include unoccupied states mainly made from H 1s orbitals,
(2) the occupied Pd d states from -0.34 to -0.21 Hartree, to which we refer as the d band in the present paper, and
(3) the occupied states below the Pd d band, to which we refer as the bottom states or the low-lying states.

Checking the O_h representation for each molecular orbital in $Pd_{13}H_x$ and Pd_{13}, we can analyse the states induced by the hydrogen adsorption. There are no significant changes in energy levels in groups (1) and (2); energy level crossover due to hydrogen adsorption does not occur near the highest occupied molecular orbital (HOMO) and the lowest unoccupied

Table 1. Various parameters at hydrogen adsorption sites of the $Pd_{13}H_6$ cuboctahedron cluster: R_H: the interatomic distance between H and the cluster-centre Pd, represented as Pd_c. R_{Pd}: the interatomic distance between Pd_c and the peripheral Pd (Pd cluster sizes). R_{H-Pd}: the interatomic distance between H and the nearest-neighbour Pd at the peripheral site. ΔE: the difference in total energy given by $E(Pd_{13}H_6) - E(Pd_{13}) - 3E(H_2)$ per H in hartrees. Second block: Mulliken's orbital populations of low-lying states. Third block: Mulliken charges. Fourth block: R_{Pd} and ΔE optimized by fixing R_H. Note the significant energy stabilization at site A′.

	Site A′	Site B′	Site D′	Site E′	Site F′
Fixed $R_{Pd} = 5.1$ au					
R_H (au)	2.87	3.45	4.87	5.56	6.26
R_{H-Pd} (au)	3.68	3.60	3.82	4.10	4.48
ΔE	−0.015	−0.080	−0.045	−0.049	−0.041
$1t_{2g}$	0.82 (Pd_c 4d)	0.66 (Pd_c 4d)	0.51 (Pd_c 4d)	0.52 (Pd_c 4d)	0.55 (Pd_c 4d)
$1t_{1u}$	0.37 (H)	0.34 (H)	0.27 (H)	0.23 (H)	0.19 (H)
$1e_g$	0.59 (Pd_c 4d)	0.38 (Pd_c 4d)	0.17 (Pd_c 4d)	0.22 (Pd_c 4d)	0.35 (Pd_c 4d)
$1a_{1g}$	0.66 (Pd_c 5s)	0.53 (Pd_c 5s)	0.32 (Pd_c 5s)	0.23 (Pd_c 5s)	0.30 (Pd_c 5s)
Mulliken charge					
H	1.24	1.26	1.16	1.13	1.08
Centre Pd	9.55	9.63	9.90	9.87	9.83
Peripheral Pd	9.92	9.90	9.92	9.94	9.97
Optimized R_{Pd}					
R_{Pd} (au)	5.40	5.24	5.20	5.18	5.06
R_{H-Pd} (au)	3.93	3.71	3.87	4.12	4.47
ΔE	−0.052	−0.088	−0.050	−0.050	−0.041

Table 2. Various parameters for hydrogen adsorption sites of the $Pd_{13}H_8$ cuboctahedron cluster: R_H, R_{Pd}, and R_{H-Pd} are the same as for table 1. ΔE: the difference in total energy given by $E(Pd_{13}H_8) - E(Pd_{13}) - 4E(H_2)$ per H in hartrees. Note that ΔE changes considerably in the relaxed case but site F is still the most stable position.

	Site A	Site B	Site C	Site D	Site F
Fixed $R_{Pd} = 5.1$ au					
R_H (au)	3.00	3.38	4.06	4.86	6.05
R_{H-Pd} (au)	3.17	3.04	2.94	3.03	3.50
ΔE	−0.001	−0.034	+0.008	−0.070	−0.081
$1a_{2u}$	0.05 (H)	0.06 (H)	0.06 (H)	0.06 (H)	0.04 (H)
$1e_g$	0.78 (Pd_c 4d)	0.64 (Pd_c 4d)	0.53 (Pd_c 4d)	0.52 (Pd_c 4d)	0.64 (Pd_c 4d)
$1t_{2g}$	0.45 (Pd_c 4d)	0.27 (Pd_c 4d)	0.11 (Pd_c 4d)	0.07 (H)	0.09 (Pd_c 4d)
$1t_{1u}$	0.35 (Pd_c 5p)	0.31 (Pd_c 5p)	0.22 (Pd_c 5p)	0.08 (H)	0.06 (H)
$1a_{1g}$	0.52 (Pd_c 5s)	0.42 (Pd_c 5s)	0.30 (Pd_c 5s)	0.08 (H)	0.05 (H)
Mulliken charge					
H	1.27	1.35	1.24	1.30	1.27
Centre Pd	8.84	8.68	9.32	9.90	10.17
Peripheral Pd	9.91	9.87	9.90	9.81	9.81
Optimized R_{Pd}					
R_{Pd} (au)	5.57	5.39	5.95	5.27	5.07
R_{H-Pd} (au)	3.57	3.27	3.52	3.10	3.50
ΔE	−0.048	−0.065	−0.064	−0.079	−0.081

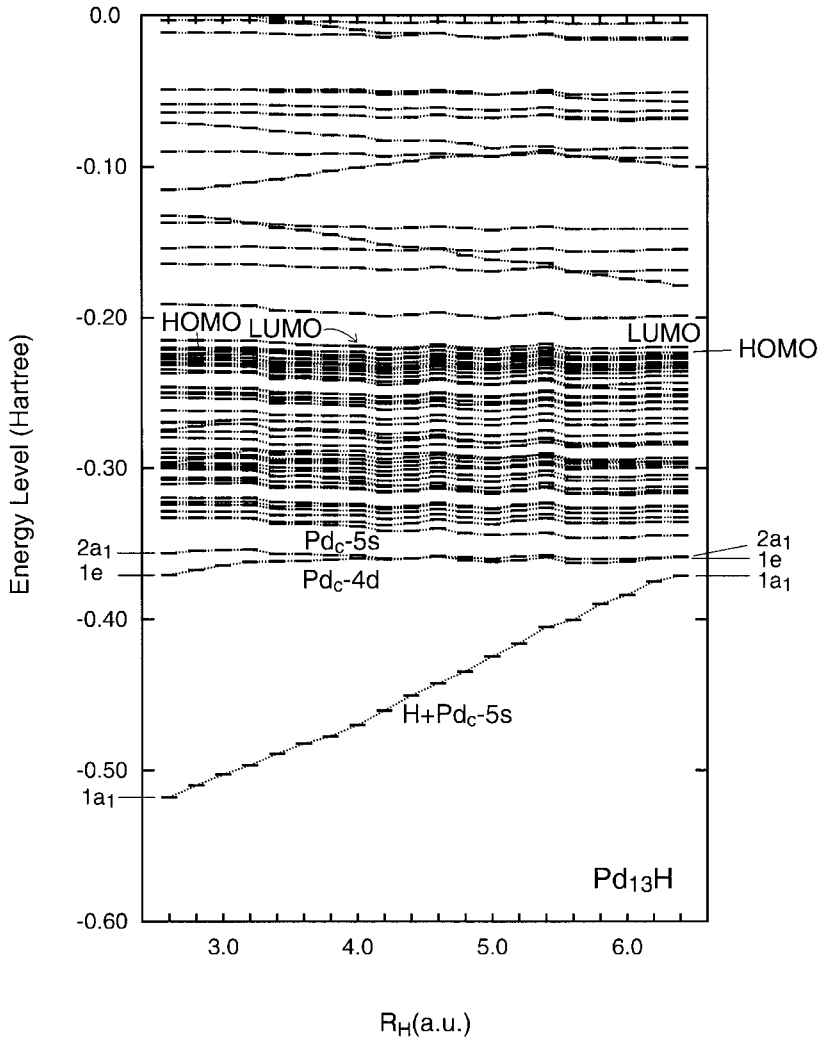

Figure 3. The change in the energy level as a function of the hydrogen position for (a) $Pd_{13}H_1$, (b) $Pd_{13}H_6$, and (c) $Pd_{13}H_8$. R_{Pd} is fixed at 5.1 au. Pd_c and Pd_p mean the centre and peripheral Pd atoms, respectively.

molecular orbital (LUMO), except for the $2a_{2u}$ state of $Pd_{13}H_8$ (figure 3(c)), so charge redistribution is not induced. In the energy levels in group (3), levels induced by the hydrogen adsorption are identified. For $Pd_{13}H_8$, the induced orbitals are the $1t_{1u}$ and $2a_{2u}$ states, although the $2a_{2u}$ orbital is unoccupied for $R_H < 4.8$ au. The induced orbitals hold the same number of electrons as those brought in by H atoms. For $Pd_{13}H_6$, the hydrogen adsorption induces the $1t_{1u}$ state in the occupied states (figure 3(b)).

The major orbital populations obtained by Mulliken population analysis are listed in tables 1 and 2 for several important states which lie among the bottom states. This analysis shows that the bottom states are strongly hybridized states of the Pd_c (the centre Pd) orbitals and the hydrogen orbitals, to which we refer as the cluster-centre states (CCSs). The Mulliken

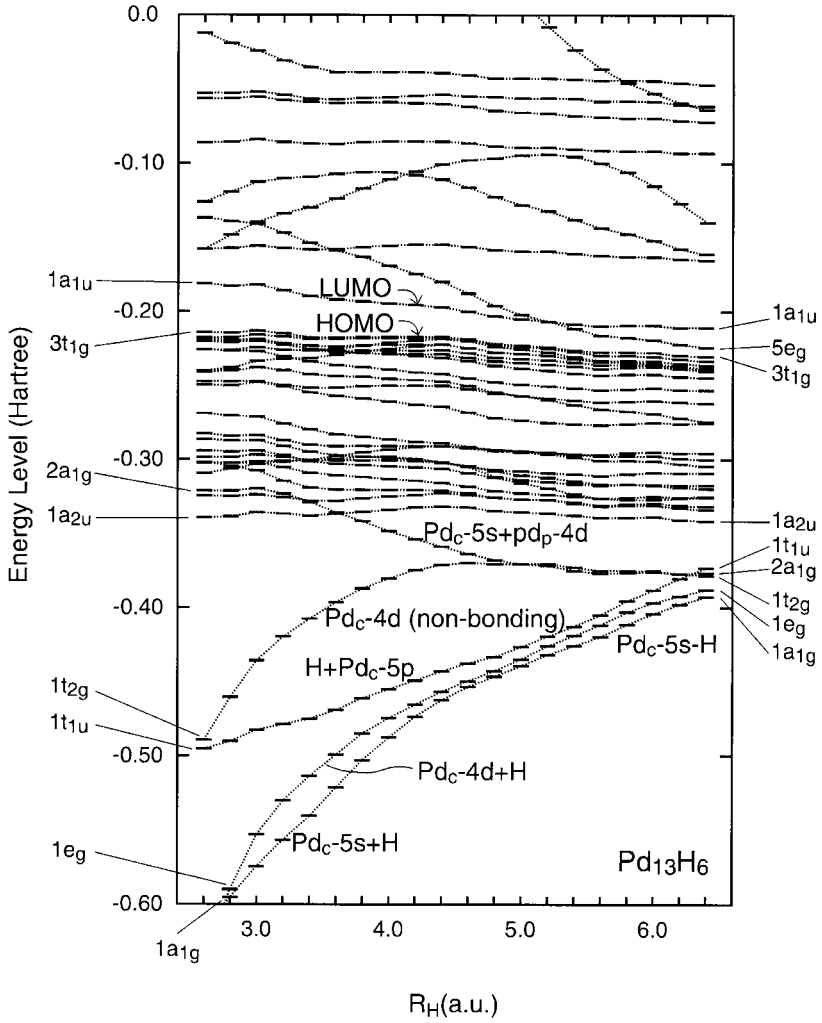

(b)

Figure 3. (Continued)

charge in tables 1 and 2 for H, which is larger than 1.0, suggests that the hydrogen atom does not lose its electron upon adsorption.

Since these hydrogen-induced bottom states mainly involve orbitals of Pd_c, we focus on the localized states near the centre. We consider the local density of states (LDOS) by expanding the eigenstates ψ_v in terms of spherical harmonics at the cluster centre as [22]

$$\psi_v(\boldsymbol{r}) = \sum_{lm} \tilde{\psi}_{vlm}(r) Y_{lm}(\boldsymbol{r})$$
$$\varrho_{vl} = \sum_m \int_0^{R_{max}} \{\tilde{\psi}_{vlm}(r)\}^2 r^2 \, \mathrm{d}r. \tag{1}$$

R_{max} is the cut-off radius which defines the centre region.

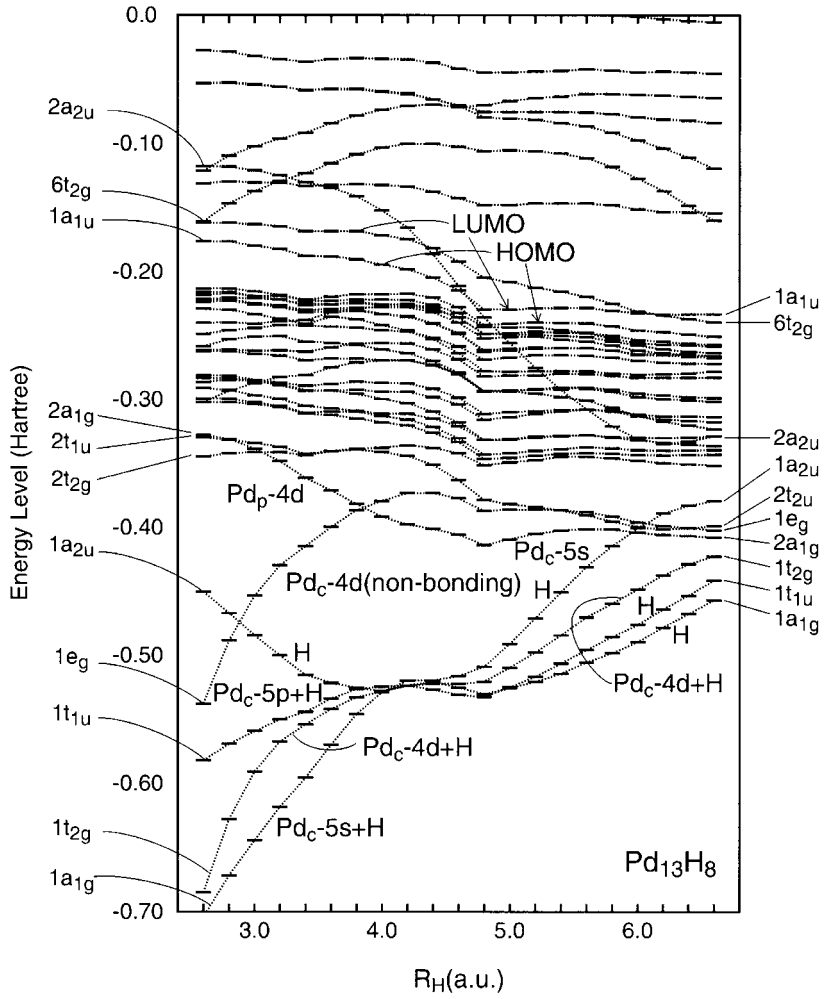

(c)

Figure 3. (Continued)

2.3. Cluster-centre states

2.3.1. Bonding and anti-bonding. In this subsection we analyse the CCSs of $Pd_{13}H_n$ with regard to the interaction between the electronic states of the peripheral Pd_{12} and those of the centre Pd_cH_n cluster.

Figure 4 shows the energy diagram for the Pd_cH_n ($n = 6, 8$), Pd_{12}, and $Pd_{13}H_n$ ($n = 6, 8$) clusters. The Pd_cH_6 cluster has a_{1g}-, e_g-, t_{1u}-, and t_{2g}-symmetry orbitals, where the t_{2g} state is non-bonding with the hydrogen orbitals. The $1t_{1u}$ HOMO and the $2e_g$ LUMO mainly comprise hydrogen 1s orbitals. The s-like a_{1g} state comprises Pd 5s and hydrogens. The Pd 4d states split into ones with t_{2g} and e_g symmetries. The LUMO is an anti-bonding state of $1e_g$ symmetry. These states interact with the states having the same symmetries in the peripheral Pd_{12} cluster. The states at the centre of the Pd_{12} cluster as calculated by equation (1) are shown in figure 5(a). The Pd_{12} cluster has electronic shell-like states including nominal numbers of $1a_{1g}$ and $1t_{1u}$

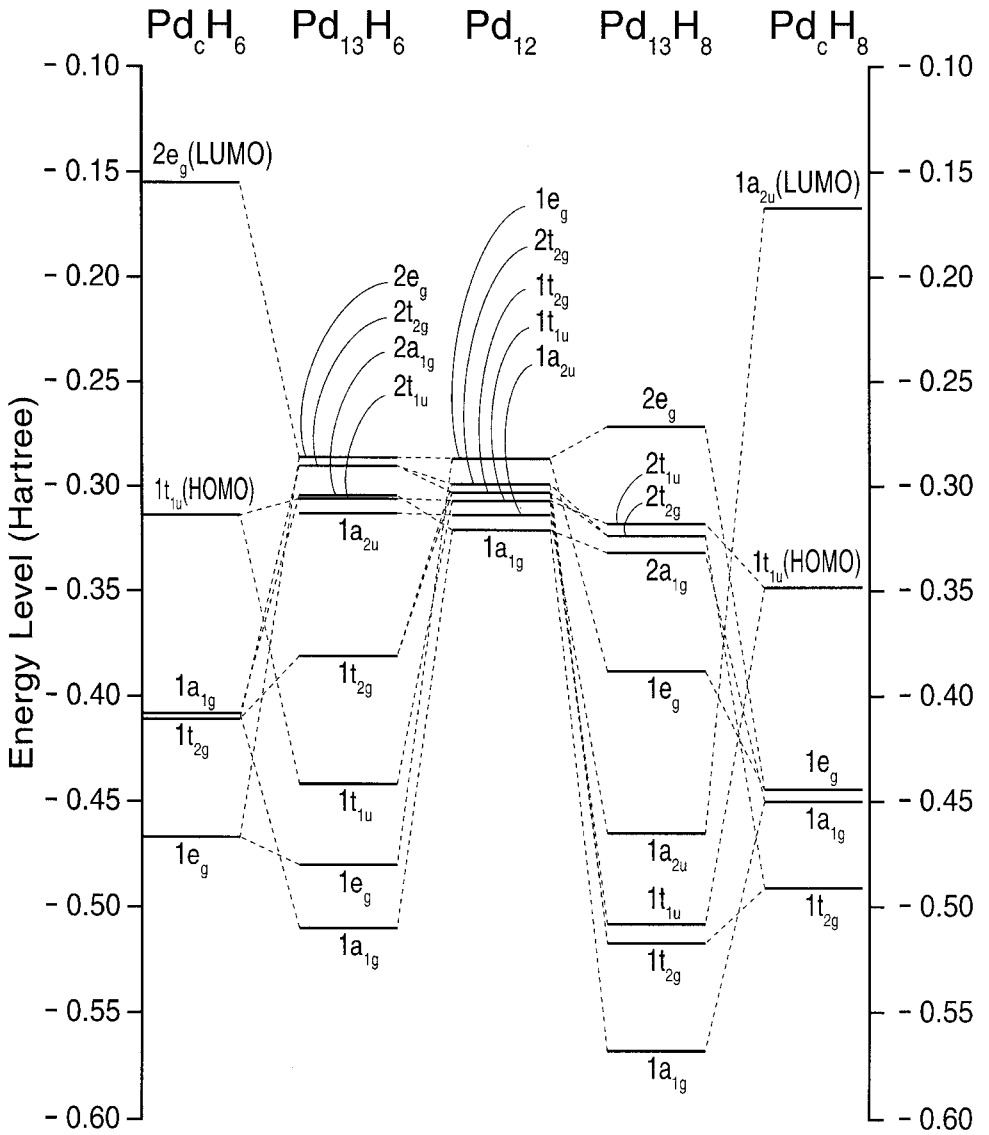

Figure 4. The energy level diagram for the low-lying levels of Pd_cH_n, Pd_{12}, and $Pd_{13}H_n$ ($n = 6, 8$) clusters.

states and a sizable number of $1a_{2u}$ states at the bottom of the d band. As is shown in figure 4, the bonding state of Pd_cH_6-$1a_g$ (the $1a_g$ state of the Pd_cH_6 cluster) with Pd_{12}-$1a_g$ is the state $Pd_{13}H_6$-$1a_g$, while anti-bonding between them produces the state $Pd_{13}H_6$-$2a_g$. The pairs of orbitals $1e_g$–$2e_g$, $1t_{1u}$–$2t_{1u}$, and $1t_{2g}$–$2t_{2g}$ for $Pd_{13}H_6$, are similarly interpreted as bonding and anti-bonding states of the Pd_cH_6 and Pd_{12} clusters. Since Pd_cH_6 has no state of a_{2u} symmetry, there is no interaction with the Pd_{12}-$1a_{2u}$ state, so the $1a_{2u}$ state has almost the same energy for Pd_{12} and $Pd_{13}H_6$. The bonding and anti-bonding nature can be seen in the energy levels of $1a_{1g}$ and $2a_{1g}$ in figure 3(b) where they change in a complementary fashion: the former goes down while the latter goes up as R_H decreases.

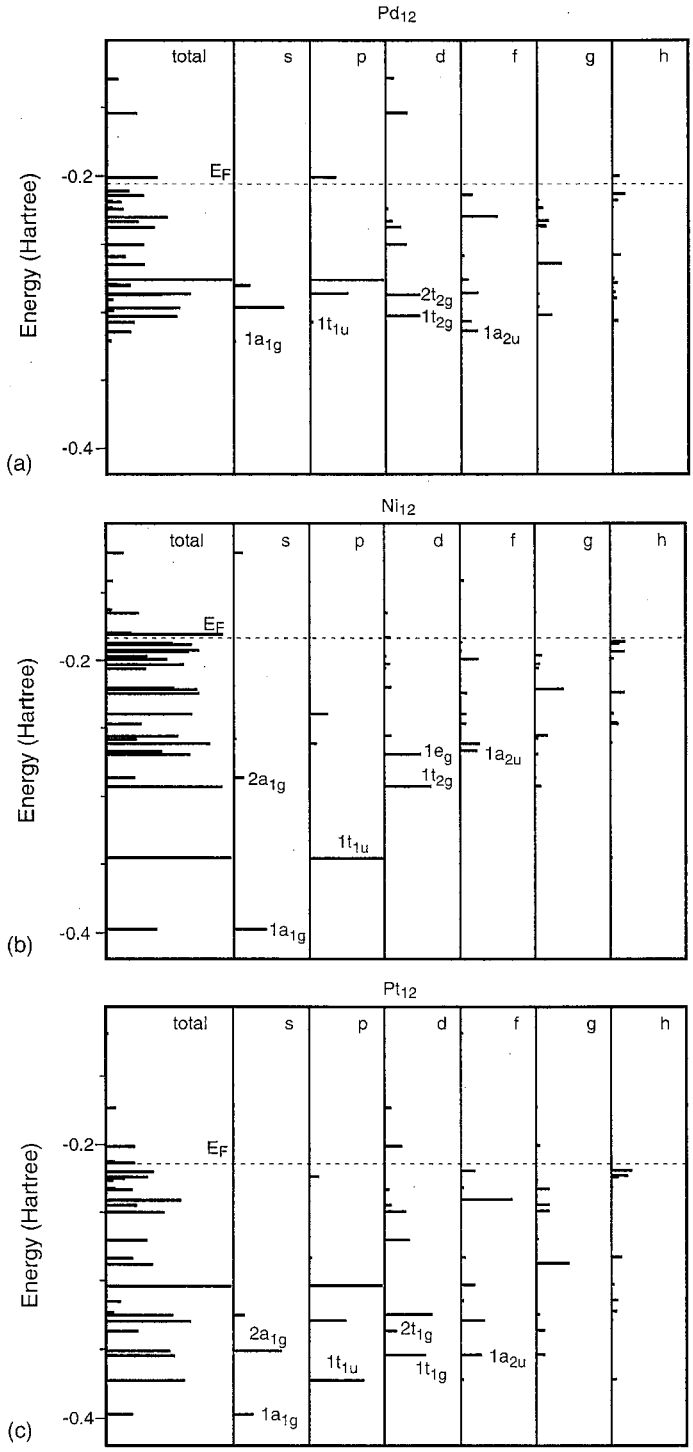

Figure 5. The energy levels and local densities of states (LDOSs) for (a) Pd_{12}, (b) Ni_{12}, and (c) Pt_{12} clusters. R_{Pd} is 5.1 au, R_{Ni} is 4.5 au, and R_{Pt} is 5.1 au. R_{max} is 3.9 au, common to all of the clusters.

In Pd_cH_8, four orbitals from the bottom have the same symmetries as those in Pd_cH_6, but the sequence of orbitals is a little changed. The HOMO t_{1u} is the same as that of Pd_cH_6 and it mainly involves the hydrogen 1s orbital. The non-bonding state is $1e_g$ for Pd_cH_8, instead of $1t_{2g}$ as for Pd_cH_6. The major difference in electronic structure from that of Pd_cH_6 is the appearance of an a_{2u} symmetry state at the LUMO. On making $Pd_{13}H_8$ from Pd_cH_8 and Pd_{12}, the Pd_cH_8-$1a_{2u}$ state is strongly hybridized with the Pd_{12}-$1a_{2u}$ state, and the energy of Pd_{12}-$1a_{2u}$ is lowered for the corresponding bonding state of $Pd_{13}H_8$-$1a_{2u}$ from -0.314 to -0.465 Hartree. The remarkable complementary shifts of bonding and anti-bonding levels for the $1a_{2u}$ and $2a_{2u}$ states in figure 3(c) are caused by the strong hybridization; the $Pd_{13}H_8$-$2a_{2u}$ state originating from Pd_{12}-$1a_{2u}$, which was one of the occupied d states of Pd_{12}, is moved to an unoccupied state upon adsorption of eight hydrogens.

In the same way the CCSs in the Pd_{13} cluster, of which the electronic structures are shown in figure 6(a), are interpreted as the states formed by bonding and anti-bonding of Pd_c and Pd_{12}. The lowest $1a_{1g}$ state of Pd_{13} is assigned as the bonding state of Pd_c 5s and Pd_{12}-$1a_{1g}$, and the anti-bonding state appears as the Pd_{13}-$2a_{1g}$ state. Since d states in the spherical symmetry split into e_g and t_{2g} representations in O_h symmetry, ten 4d electrons in the Pd_c atom split into $1e_g$ and $1t_{2g}$ states. Therefore mainly Pd_{12}-$1e_g$ and Pd_{12}-$1t_{2g}$ states are stabilized by the Pd_c–Pd_{12} interaction; however, the energies of these bonding states (>-0.358 Hartree) are much higher than the H 1s energy (-0.5 Hartree).

2.3.2. Comparison with Ni and Pt. It is of interest to compare the energy levels and LDOSs of Pd_{12}, Pd_{13}, and $Pd_{13}H_n$ with those of Ni_{12}, Pt_{12}, Ni_{13}, and Pt_{13} which cannot be used for hydrogen storage. In figures 5(a), 5(b), and 5(c) the LDOSs of Pd_{12}, Ni_{12}, and Pt_{12} derived using equation (1) are shown, respectively, for $R_{max} = 3.9$ au. In figure 5(a), the low-lying states of Pd_{12}, $1a_{1g}$, $1t_{1u}$, and $1a_{2u}$, show only a nominal DOS and are located almost in the d band from -0.35 to -0.2 Hartree, while in figure 5(b) for Ni_{12} the states seem to fall into two categories: one is the d band states (-0.27 to -0.18 Hartree) and the other is the states constituting a shell-like structure (-0.4 to -0.28 Hartree). In Pt_{12} (figure 5(c)), the lowest two states show a shell-like structure and the boundary with the d band is not clear.

The energy levels of Pd_n, Ni_n, and Pt_n ($n = 12, 13$) together with Pd_cH_n, Ni_cH_n, and Pt_cH_n ($n = 6, 8$) are shown in figure 6. The lowest state has a_{1g} symmetry in all three clusters. As already discussed for Pd_{12} and Pd_cH_n clusters, this state in Ni_{12} and Pt_{12} will interact with $1a_{1g}$ states of Ni_cH_n, and Pt_cH_n clusters, as expected from the data shown in figures 6(b) and 6(c). The $1a_{1g}$ state for both Ni_{12} and Pt_{12} clusters is at about -0.4 Hartree which is close to the H 1s energy (-0.5 Hartree), as compared to the level of Pd_{12}-$1a_{1g}$, -0.32 Hartree. On the other hand, the $1a_{1g}$ state of the core cluster—Ni_cH_6-$1a_{1g}$, Ni_cH_8-$1a_{1g}$, Pt_cH_6-$1a_{1g}$, and Pt_cH_8-$1a_{1g}$—is also the lowest state and has a level lower than -0.42 Hartree, as shown in figure 6. This implies that the interaction between the Ni_cH_n (or Pt_cH_n) and the peripheral Ni_{12} (or Pt_{12}) is stronger than that in Pd_cH_n and Pd_{12}. Recalling that the energy of $1a_{1g}$ of Ni_{12} or Pt_{12} is less than -0.4 Hartree, the energies of the $1a_{1g}$ states of $Ni_{13}H_n$ and $Pt_{13}H_n$ may be much lower than -0.5 Hartree and the anti-bonding states $2a_{1g}$ may change d-band states in $Ni_{13}H_n$ and $Pt_{13}H_n$ clusters, like the $2a_{2u}$ case for the $Pd_{13}H_8$ cluster. This is energetically unfavourable for hydrogen adsorption. Further, in Ni_{12}, the $1a_{1g}$ state has 1.08 electrons and $1t_{1u}$ state has 2.48 electrons in the region inside R_{max} (=3.9 au) although there is no atom at the cluster centre. In Pd_{12} the $1a_{1g}$ state has 0.02 electrons and $1t_{1u}$ state has 0.05 electrons in the same region. In Pt_{12} the $1a_{1g}$ state has 0.26 electrons and $1t_{1u}$ state has 0.68 electrons in the same region. There are thus 50 times more electrons in the centre region in Ni_{12} than in the Pd_{12} cluster. That is, the electronic states of NiH_n and the states at the centre of Ni_{12} clusters have large spatial overlap.

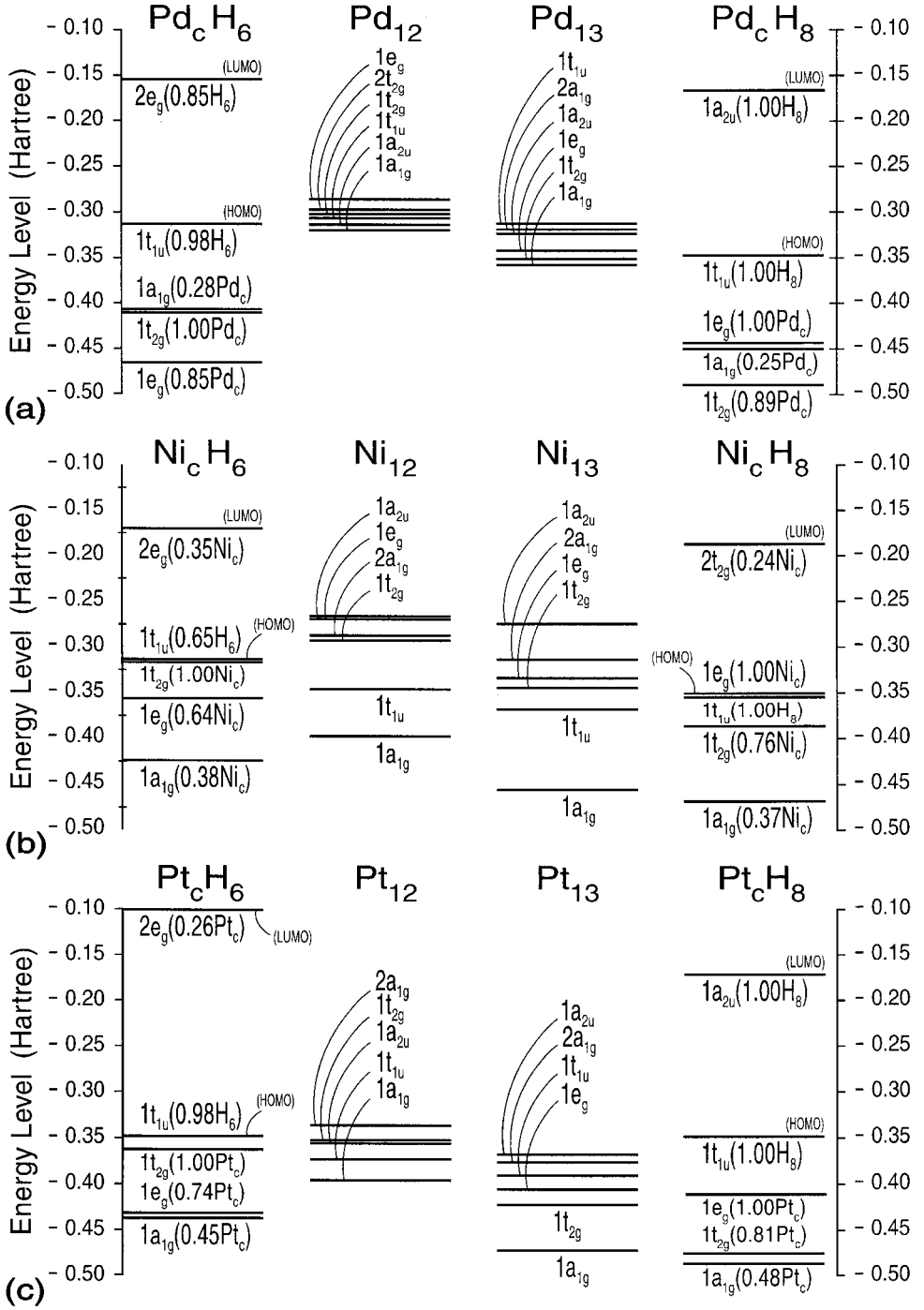

Figure 6. Energy levels for (a) Pd, (b) Ni, and (c) Pt clusters. For Pd_cH_n, Ni_cH_n, and Pt_cH_n ($n = 6, 8$) clusters, Mulliken's orbital populations are indicated. R_{Pd} is 5.1 au, R_{Ni} is 4.5 au, and R_{Pt} is 5.1 au.

2.3.3. Charges of cluster-centre states. Since the properties of the electronic shell structure around the centre atom can be described using the LDOS, we calculate the LDOSs for Ni_{13}, Pd_{13}, and Pt_{13} by using equation (1). The value of R_{max} is set such that the sum of the LDOSs becomes 5, corresponding to ten electrons. In table 3 the total LDOS defined as

$$\varrho_l^{(\mathrm{total})} = \sum_{\nu=\mathrm{occupied}} \varrho_{\nu l}$$

and the LDOSs for the lowest CCSs

$$\varrho_l^{(\mathrm{low-lying})} = \sum_{\nu=\mathrm{low-lying}} \varrho_{\nu l}$$

are tabulated together with R_{max}. The deviation of the total LDOS from the sum of s, p, d, and f LDOSs is due to higher-angular-momentum components. Ni_{13} and Pt_{13} have larger 1s and 1p components than Pd_{13}. In contrast, for 1d states, Pd_{13} has slightly more electrons than Ni_{13} and Pt_{13}. Hydrogen states adsorbed in metal clusters mainly composed of 1s and 1p states are easily introduced in Pd_{13}, where the LDOSs for s and p are small, compared with those in Ni_{13} or Pt_{13}.

Table 3. Sums of the LDOSs of three low-lying states for Ni_{13}, Pt_{13}, and $Pd_{13}H_n$.

		Total LDOS					Low-lying states		
Cluster	R_{max} (au)	Total	s	p	d	f	1s	1p	1d
Ni_{13} ($R_{Ni} = 4.46$)	2.42	5.00	0.38	0.38	4.19	0.03	0.38	0.38	4.19
Pt_{13} ($R_{Pt} = 5.1$)	2.82	5.00	0.40	0.35	4.15	0.07	0.40	0.35	4.15
Pd_{13} ($R_{Pd} = 5.1$)	2.78	5.00	0.31	0.23	4.39	0.05	0.30	0.23	4.39
$Pd_{13}H_6$ ($R_{Pd} = 5.24$)	3.62	7.99	0.63	1.14	5.18	0.51	0.63	1.12	3.37
$Pd_{13}H_8$ ($R_{Pd} = 5.39$)	3.70	8.98	0.66	1.29	5.47	0.74	0.66	1.28	3.14
$Pd_{13}H_{6+8}$ ($R_{Pd} = 5.5$)	4.02	12.01	0.80	1.95	6.45	1.36	0.80	1.95	3.73

To clarify the state of the valence electrons of hydrogen, we calculate LDOSs for $Pd_{13}H_6$, $Pd_{13}H_8$, and $Pd_{13}H_{6+8}$, in which the centre Pd has ten electrons and the adsorbed hydrogens six, eight, and fourteen electrons, respectively (table 3).

For $Pd_{13}H_6$, $1a_{1g}$ (1s), $1e_g$ (1d), $1t_{1u}$ (1p), and $1t_{2g}$ (1d) constitute the CCSs. According to table 3, the total number of electrons in the low-lying 1s, 1p, and 1d states amounts to 10.3 electrons, while the remaining 5.7 electrons belong to the d band. It should be noted that the total LDOS for s symmetry is fully explained by that of the 1s state (0.63). The s and p symmetries come from the 1s and 1p states. This indicates that the 1s and 1p states in $Pd_{13}H_6$ are just the core-like states.

For $Pd_{13}H_8$, $1a_{1g}(1s)$, $1t_{2g}(1d)$, $1t_{1u}(1p)$, $1a_{2u}(1f)$, and $1e_g(1d)$ constitute the CCSs. In total, in these low-lying states there are 10.8 electrons in the centre sphere of $R_{max} = 5.39$ au. Also in this case, the 1s and 1p states of the CCSs are core-like states. The s and p components of the CCSs are located below the d band. The probability density for the $1a_g$ state is spatially distributed in the volume of the sphere with radius R_{max} to a level of 66% and that for $1t_{1u}$ state is localized in this region to a level of 43%. Similar analysis for $Pd_{13}H_{6+8}$ shows that the states with s or p symmetry are located below the 4d band, and the probability density for the $1a_g$ state is localized in the sphere with $R_{max} = 5.5$ au to a level of 82% and that for the $1t_{1u}$ state to a level of 65% (table 3). The CCSs are the cluster-shell-like states located below the Pd d band and loosely localized spatially near the cluster centre.

3. Cluster decomposition of the fcc lattice

Recently, there have been several attempts to create new materials as cluster-assembled solids based on the well defined local electronic structure of the unit cluster [28,29]. It is empirically known that the lattice structure of fcc metals is well described by the 13-atom-cuboctahedron cluster. In addition, the fcc lattice can be expressed as the lattice of the 13-atom-cuboctahedral cluster, as shown in figure 7(a). This indicates that the fcc lattice can be regarded as a cluster-assembled solid. The unit cell of this cluster lattice is rhombohedral with the fundamental lattice vectors (3, 0, −1), (−1, 3, 0), and (0, −1, 3), where (1, 1, 0), (0, 1, 1), and (1, 0, 1) are those for the fcc lattice. The space group for this rhombohedral crystal is $R\bar{3}$ and the positions of the atoms are tabulated in table 4. At a stoichiometric concentration of PdH, hydrogen atoms are believed to occupy the o-sites. We also give expressions for the octahedral sites in the fcc crystal in terms of the rhombohedral cell partitioning of an fcc lattice.

Table 4. Atom positions in the rhombohedral unit cell.

Atom	(t_1, t_2, t_3)	Wyckoff symbol
Pd(1)	(0, 0, 0)	1a
Pd(2)	(6/13, 5/13, 2/13)	6f
Pd(3)	(3/13, 9/13, 1/13)	6f
H(1)	(1/2, 1/2, 1/2)	1b
H(2)	(11/26, 7/26, 21/26)	6f
H(3)	(9/26, 1/26, 3/26)	6f

In the rhombohedral cluster lattice, there exist three geometrical configurations for the nearest-neighbouring cluster as shown in figures 7(b), 7(c), and 7(d). The first one is along the body-diagonal direction of the unit cell shown in figure 7(b). The distance between the two clusters is 2.449 times the nearest Pd–Pd distance (13.76 au) in the crystal. The second one is along the edge direction and separated from the central one by 2.236 times the Pd–Pd distance, indicated by the square in figure 7(a) and shown in figure 7(c). The third case is along the face-diagonal direction of the unit cell as shown in figure 7(d). The inter-cluster distance is 2.646 times the Pd–Pd distance. Interpreting the fcc crystal as the lattice of the cuboctahedron clusters provides us with a new approach to discussing electronic structures of complex systems.

If one assumes the Pd(1) site as the centre of a cuboctahedron, H(1) and H(2) sites are along the threefold axes of the cuboctahedron and close to the F site for the $Pd_{13}H_8$ cluster whereas H(3) sites are centres of square faces of the cuboctahedron, which correspond to B′ sites for the $Pd_{13}H_6$ cluster. So the superstructures Pd/H(1) + H(2) and Pd/H(3) can be viewed as assemblies of the $Pd_{13}H_8$ and $Pd_{13}H_6$ clusters, respectively.

We calculate the electronic structures for these hypothetical crystals by using the linearized muffin-tin orbital method in the atomic sphere approximation (LMTO-ASA). Figures 8(a), 8(b), and 8(c) show DOSs of the bulk systems Pd, Pd/H(3), and Pd/H(1) + H(2), respectively. The electronic structures of Pd_{13} agree quite well with the bulk DOS of Pd metal except as regards the states at the band bottom. It is remarkable that the DOS of Pd/H(3) agrees very well with that of $Pd_{13}H_6$, because the H atoms are inside the cluster. The isolated $Pd_{13}H_6$ cluster can represent bulk electronic structures. Although the DOS of the Pd/H(1) + H(2) system does not change much from that of Pd/H(3), the energy levels of $Pd_{13}H_8$ are different from those of the bulk crystal because the 1s states of H in $Pd_{13}H_8$, being outside the cluster, lie higher than the bulk state.

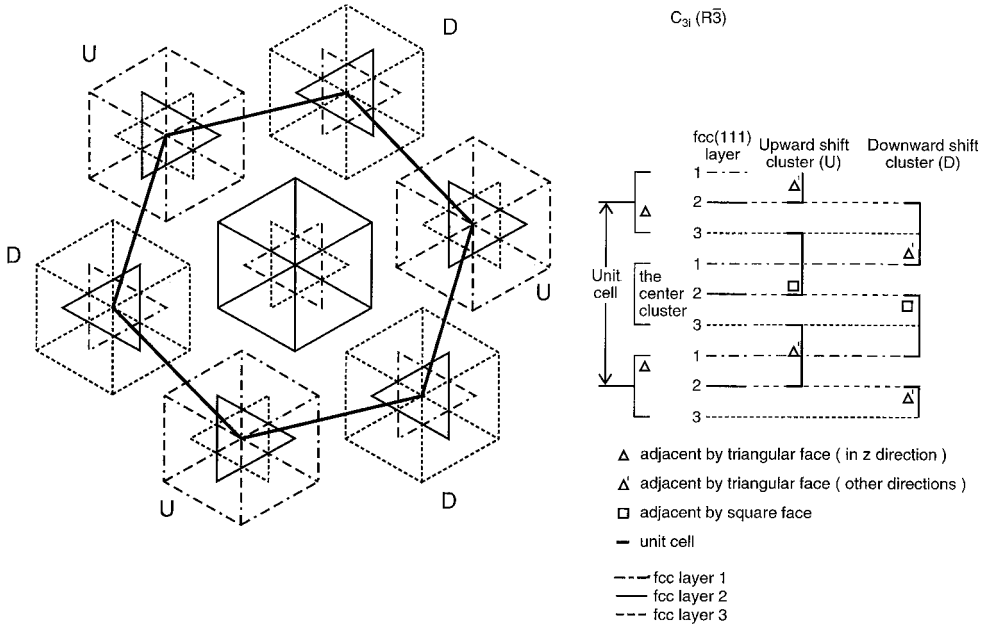

(a)

Figure 7. (a) An fcc bulk as a crystal of cuboctahedron clusters. The rhombohedral cell is shown in hexagonal view. The left-hand panel shows the decomposition in the xy-plane and the right-hand panel shows that in the z-direction. The three types of fcc mesh in the (111) face are indicated by a dot–dash line, a solid line, and a dashed line. The relations between the centre cluster and the surrounding clusters are indicated by $\triangle$, $\triangle'$, and $\square$ in the right-hand panel. (b), (c), (d) Three types of inter-cluster relation in the crystal of cuboctahedron clusters. (b), (c), and (d) correspond to $\triangle$, $\square$, and $\triangle'$ shown in (a), respectively.

4. Discussion

4.1. The 13-atom cuboctahedron as an elementary cluster

Hydrogen adsorption into the 13-atom-cuboctahedron cluster has two characteristic features which are similar to those of the bulk:

(i) The 13-atom-cuboctahedron cluster has two types of site at which hydrogen can adsorb; one corresponds to the o-site and the other to the t-site in the bulk. Occupation of the latter in the cluster by hydrogen atoms causes a remarkable expansion of the Pd–Pd distance, which is similar to that in the β-phase in bulk PdH.

(ii) The electronic structures of $Pd_{13}H_n$ clusters agree well with those of bulk PdH, when the hydrogen atoms are inside the Pd_{13} cluster.

Thus the 13-atom-cuboctahedron cluster describes bulk states, as its centre atom interacts with all the nearest neighbours in the fcc lattice. Furthermore, the metallic nature of the bonding is free from the effect of dangling bonds—compared with the covalent bond which has a bonding direction and the ionic bond which has polarity. In addition to the above similarity, the fcc bulk is divided into 13-atom-cuboctahedron clusters without absence or overlap of the atoms. Assuming that the bulk PdH can be described with $Pd_{13}H_n$ clusters, we shall estimate the entropy change at the phase transition of the bulk PdH in the next subsection. In this section, to clarify how large a cluster is needed to reveal the elementary character of bulk solid,

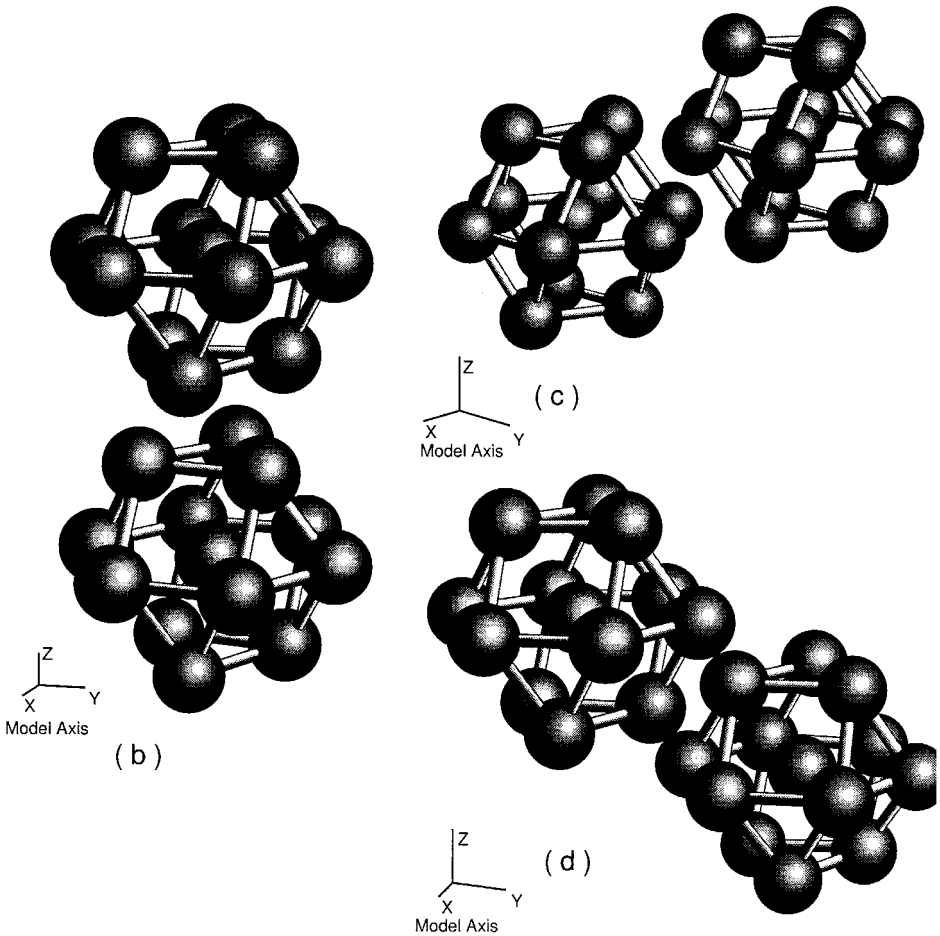

(b)

Figure 7. (Continued)

we investigate small sub-clusters, a triangular Pd_3H sub-cluster, a square Pd_4H sub-cluster, a triangular-pyramid Pd_cPd_3H sub-cluster, and a square-pyramid Pd_cPd_4H sub-cluster, in which the Pd structure is a part of a 13-atom-cuboctahedron cluster.

First we examined the total-energy change as a function of the hydrogen distance from the small cluster face. For planar Pd sub-clusters there is one minimum for hydrogen adsorption, at $R_H = 6.36$ au for Pd_3H and $R_H = 7.62$ au for square Pd_4H. Here the distance R_H represents the distance from the centre of the virtual 13-atom-cuboctahedron cluster. These distances are longer than those of the sites F and F′ for the Pd_{13} cluster. Even at the minimum position for square Pd_4H, however, the total energy is positive, indicating that the hydrogen atom is never bound. For pyramid clusters there are two minima: one is inside $R_H = 3.16$ au for Pd_cPd_3H and $R_H = 2.07$ au for Pd_cPd_4H, and the other is outside $R_H = 6.16$ au for Pd_cPd_3H and $R_H = 7.48$ au for Pd_cPd_4H, where the tops of the pyramids correspond to the Pd_c of $Pd_{13}H_n$. The hydrogen atom is not bound at the inside minimum site for Pd_cPd_4H. The minimum sites inside the pyramids are close to the sites A and A′ and those outside the pyramids to sites F and F′. This implies that the sites A, A′, F, and F′ in the cuboctahedron cluster are almost

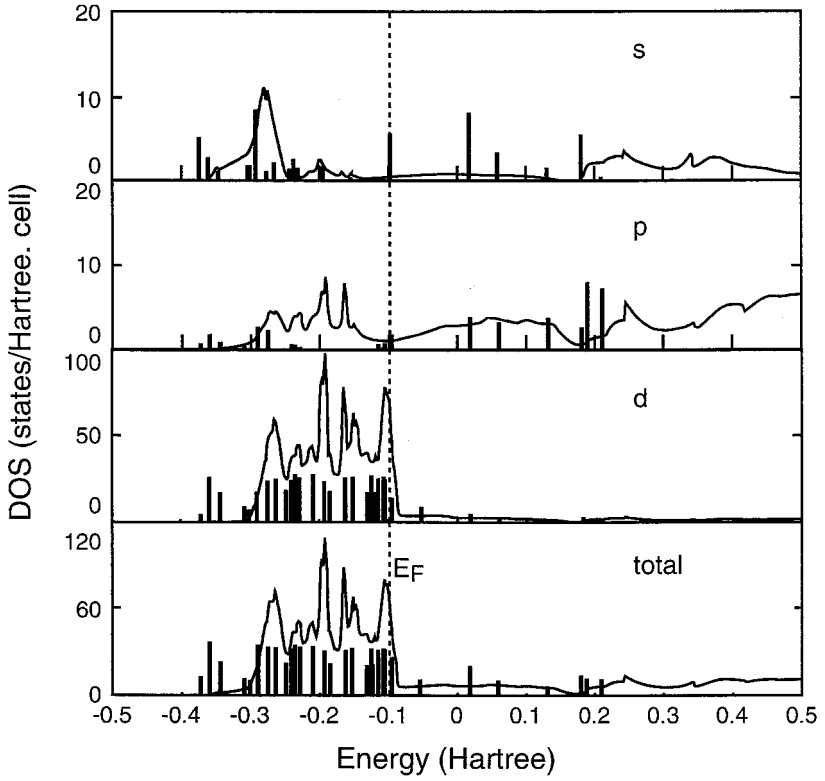

(a)

Figure 8. The energy levels and the densities of states (DOSs) for (a) Pd_{13}, (b) $Pd_{13}H_6$, and (c) $Pd_{13}H_8$ clusters, together with their corresponding bulk crystals. In each case, the histogram indicates the results for the clusters and the continuous line indicates the results of LMTO band calculations for the corresponding bulk crystals.

determined by the interaction of the H atom with the pyramidal sub-cluster. However, the most stable hydrogen site, B′, corresponding importantly to the o-site in the bulk, and the sites other than A′, F′, A, and F never appear in these sub-clusters.

There are three states relevant to the hydrogen atom in these sub-clusters:

(1) an H 1s and Pd 4d hybridization state;
(2) an H 1s and Pd 5s bonding state; and
(3) an H 1s and Pd 5s anti-bonding state.

In the Pd_3H and Pd_cPd_3H clusters, the state (1) becomes the lowest one and, especially in the triangular-pyramid cluster, it has an energy level close to the H 1s one. In both clusters the states (2) and (3) are not occupied. In Pd_4H and Pd_cPd_4H, the state (1) is not formed and the states (2) and (3) are occupied. As the anti-bonding state is occupied, hydrogen is not bound to the square cluster. In the Pd_cPd_4H cluster, the states (1) and (2) are occupied, and the state (2) is lower than the state (1). Since there is no state which has an energy level close to the H 1s one, Pd_cPd_4H is less stable than Pd_cPd_3H.

In the Pd_{13} cuboctahedron clusters, there are also three types of state relevant to hydrogen adsorption:

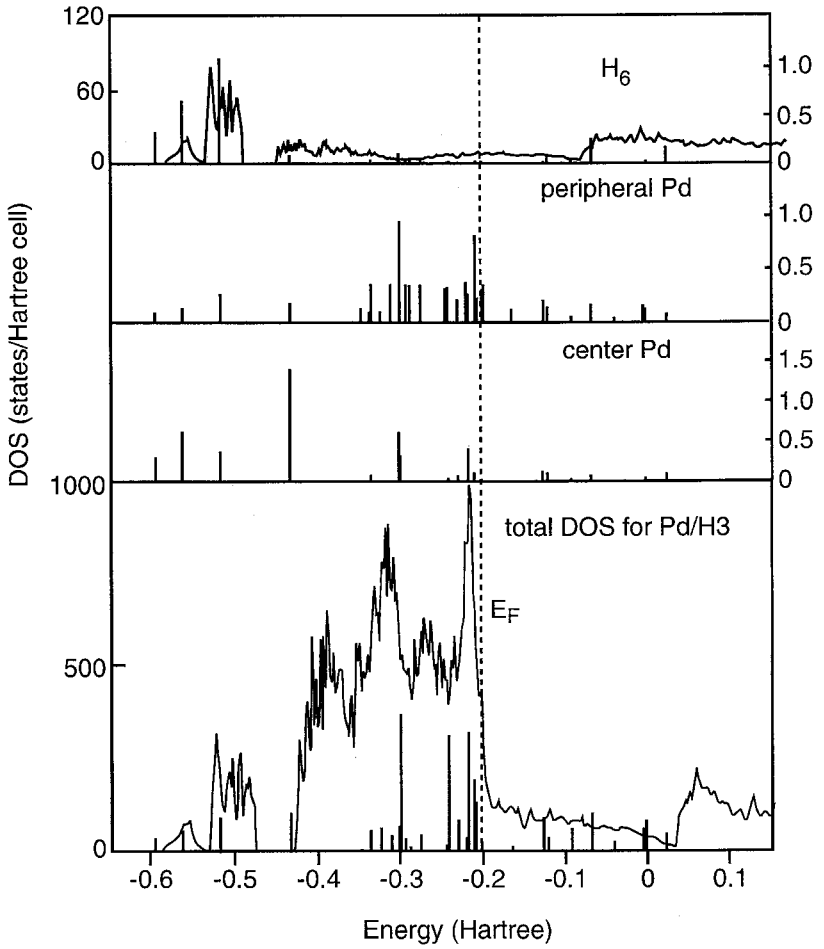

(b)

Figure 8. (Continued)

(I) H 1s and peripheral Pd 4d hybridization states;
(II) H 1s and Pd_c (5s or 4d) bonding states;
(III) H 1s and Pd_c (5s or 4d) anti-bonding states.

The states (I), (II), and (III) correspond to those of (1), (2), and (3) for the sub-clusters, respectively. That is, the peripheral Pd 4d of the Pd_c orbitals in the Pd_{13} cuboctahedron cluster take a role similar to that of the Pd 4d or Pd 5s ones in the sub-clusters. Furthermore, the bonding state (II) of the centre atom and the hydrogen atoms becomes more dominant in the states relevant to hydrogen adsorption than the hybridized state (I), and the energy levels of the states relevant to hydrogens are lowered close to the H 1s energy. Pd_c plays an important role in the Pd_{13}/H systems. The 13-atom-cuboctahedron cluster is the smallest cluster that has the pseudo-spherical symmetry and the elementary character of the bulk.

Since $Pd_{13}H_n$ ($n = 6, 8$) cuboctahedron clusters have been restricted to the O_h symmetry in the present calculations, there may be additional distortion caused by the Jahn–Teller effects because of the degeneracy at the HOMO in $Pd_{13}H_6$. The Jahn–Teller effects for Pd_{13} and Pt_{13}

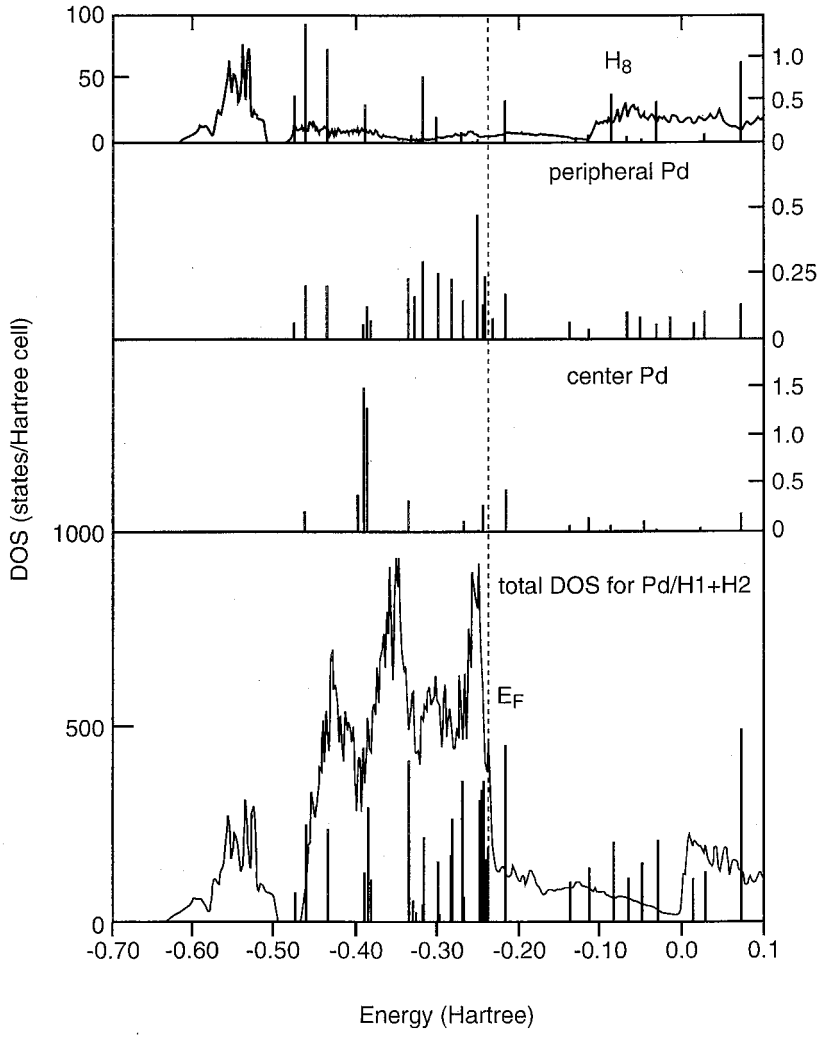

(c)

Figure 8. (Continued)

were fully discussed in our previous work [22]; the energy change induced by the Jahn–Teller distortion is an order of magnitude less than that induced by spin polarization or spin–orbit coupling effects. Since the HOMO comprises mainly Pd 4d states in $Pd_{13}H_n$ ($n = 6, 8$) and the low-lying states play an essential role in the hydrogen adsorption, the Jahn–Teller effect and the other two effects which are also associated with electronic states near the HOMO and LUMO are not significant in the present case.

4.2. The single-cluster model for bulk PdH_x

4.2.1. α- and β-phases. The cluster decomposition scheme given in section 3 provides us with a clue as to the hydrogen configuration in both the α- and β-phases so long as the Pd atoms keep the fcc structure in both phases. Bulk Pd with the hydrogen concentration x is

represented as PdH_x. Since x in the α-phase is very small, the α-phase is represented by an aggregate of $Pd_{13}H_n$ and Pd_{13} clusters with a ratio $1{:}\nu$ as $Pd_{13}H_n + (Pd_{13})_\nu$, where x is related to ν as follows:

$$x = \frac{n}{13}\frac{1}{1+\nu}.$$

At $x = 0.011$, ν is 6, 41, and 55 for $n = 1$, 6, and 8 respectively, for example. Since the most stable hydrogen sites in Pd_{13} are the B′ and F sites (o-sites) [5], we assume that the α-phase can be modelled by Pd_{13} with a few hydrogen atoms at such o-sites as B′ or F sites. In the case of higher concentration, because ν becomes negative when $n \leqslant 7$ at $x = 0.6$, the β-phase is not modelled by the mixture $Pd_{13}H_n + (Pd_{13})_\nu$. To investigate the α–β transition which occurs for $x \approx 0.6$, the β-phase is modelled by a $Pd_{13}H_8$ cluster.

As we have shown in section 2, the o-site in the fcc lattice corresponds to the B′ site inside the square face and the F site outside the triangular face of the 13-atom cluster, and the t-site in the fcc lattice corresponds to either B or C sites inside the triangular face of the 13-atom-cuboctahedron cluster. There are 13 o-sites for each 13-atom-cuboctahedron cluster, i.e., six sites of B′ type and seven sites of F type, where two of the F sites on the z-axis shown in figure 7(a) are shared by the upper and lower clusters. Since the number of o-sites is equal to the number of Pd atoms in the fcc lattice, the o-sites in the 13-atom cluster account for all of the o-sites in the fcc lattice, i.e., o-sites in the fcc lattice are completely decomposed into the 13-atom-cuboctahedron cluster without absence or overlap of o-sites. On the other hand, the number of t-sites for one Pd atom in the fcc lattice is 2. Therefore the number of t-sites for thirteen Pd atoms is 26, while the number of t-sites inside the 13-atom-cuboctahedron cluster is 8. We consider here only the eight t-sites (B or C sites) around Pd_c, on the basis of the spherically symmetrical nature of the CCSs.

Let us focus our discussion on the hydrogen site in $Pd_{13}H_8$ of the β-phase. From the energetics for the cluster in the previous sections and the literature [5], hydrogens occupy the o-sites in the α-phase (the o-site model). Because the B site is a second candidate site for hydrogen adsorption, the newly occupied site in the β-phase is thought to be a B site (the ot-site model). The t-site occupation in the $Pd_{13}H_8$ cluster predicts an appropriate lattice expansion of the bulk β-phase; this is because hydrogens at the t-sites require much more space than ones at the o-sites to keep an appropriate interatomic distance, as discussed in section 3. This is also indicated by the bulk PdH induced by lattice relaxation as described by Elsässer *et al* [10]. To estimate the entropy change in the α-to-β phase transition of bulk PdH, we calculate the entropy difference between the o-site and ot-site models:

$$\Delta S = k_B \ln W_\beta / W_\alpha = k_B \ln W_{\mathrm{ot}} / W_{\mathrm{o}}$$

where W_{ot} and W_{o} are the numbers of distinguishable states. The following three assumptions are adopted in making this estimate:

(1) the B′ site and F site are equivalent as o-sites;
(2) bulk Pd near the transition is approximated by a $Pd_{13}H_8$ cluster;
(3) we assume that the adsorption energy depends only on the site (o-site or t-site) at which the hydrogen atom adsorbs, although this energy may depend on the hydrogen configuration.

W_{o} is given by ${}_{13}C_8$ (=1287), while W_{ot} is a little complicated. The o-site and t-site, which are outside and inside of the same triangular face of the 13-atom cluster, respectively, are not occupied simultaneously because of the H–H repulsion. As listed in table 5, we calculate W_{ot} as 7260 for $Pd_{13}H_8$, in which one H atom is assumed to be at the t-site and the other seven H atoms are at o-sites (sites B′ or sites F).

Table 5. The number of distinguishable hydrogen configurations for the ot-site model.

Occupied F(z) site	Occupied F sites	Occupied B′ sites	Possible t-sites	Distinguishable states
1	0	6	7	${}_6C_0 \times {}_6C_6 \times 7 = 7$
1	1	5	6	${}_6C_1 \times {}_6C_5 \times 6 = 216$
1	2	4	5	${}_6C_2 \times {}_6C_4 \times 5 = 1125$
1	3	3	4	${}_6C_3 \times {}_6C_3 \times 4 = 1600$
1	4	2	3	${}_6C_4 \times {}_6C_2 \times 3 = 675$
1	5	1	2	${}_6C_5 \times {}_6C_1 \times 2 = 72$
1	6	0	1	${}_6C_6 \times {}_6C_0 \times 1 = 1$
0	1	6	7	${}_6C_1 \times {}_6C_6 \times 7 = 42$
0	2	5	6	${}_6C_2 \times {}_6C_5 \times 6 = 540$
0	3	4	5	${}_6C_3 \times {}_6C_4 \times 5 = 1500$
0	4	3	4	${}_6C_4 \times {}_6C_3 \times 4 = 1200$
0	5	2	3	${}_6C_5 \times {}_6C_2 \times 3 = 270$
0	6	1	2	${}_6C_6 \times {}_6C_1 \times 2 = 12$
Total:				7260

Thus, $T\ \Delta S$ for $T = 293$ K is given in hartrees as follows:

$$T\ \Delta S = 293\, k_B \log \frac{7260}{1287} \approx 0.002.$$

This value for $T\ \Delta S$ is comparable with ΔH estimated from the differences in energies per H of the local minima for H adsorption. From tables 1 and 2, the value of ΔH is estimated to be 0.023 Hartree using the binding energies per H for the sites B′ and B. Since these two sites are inside the 13-atom cluster, the binding energies are thought to be good approximations of those in the bulk. However, this ΔH is ten times larger than $T\ \Delta S$. Since ΔE per H for site B′ in table 1 (-0.088 Hartree) agrees well with the experimental enthalpy of formation for PdH (-2.2 eV $= -0.080$ Hartree) [27], this discrepancy is thought to arise from the underestimation of the binding energy ($-\Delta E$ per H) of site B ($0.065 = -(-0.065)$ Hartree). The binding energy for $Pd_{13}H_8$ is underestimated if H atoms are placed at the same sites. We will discuss this total-energy dependence on the number of H atoms in the next subsection. So we have optimized $Pd_{13}H_6$ for B sites, and the binding energy is obtained as 0.083 Hartree at $R_H = 3.4$ au and $R_{Pd} = 5.43$ au. This value of R_{Pd} suggests the expansion of the Pd–Pd distance to a similar degree to that in the β-phase. ΔH becomes 0.005 Hartree, from these binding energies, which is of the same order as the value of the estimated $T\ \Delta S$, though it is still 2.5 times larger than $T\ \Delta S$. We also note that the configuration entropy for the o-site model as a function of n, ${}_{13}C_n$, decreases monotonically for $n \geqslant 8$.

It is known that the ratio of the number of hydrogen atoms to that of Pd atoms in Pd bulk cannot be represented by a simple integer. For example, transition behaviour appears in the pressure–composition–temperature curve for PdH_x at $x = 0.075$, 0.46, and 0.61 [5]. It is interesting that these decimals can be represented by fractions of 13: that is, $1/13 = 0.0769$, $6/13 = 0.461$, and $8/13 = 0.615$, respectively. Further, while the phase diagrams for bcc metal hydrides (VH, NbH, TaH, etc) show very complicated phases [5], PdH has only two phases. We speculate that this is because just one species of cluster, i.e., the cuboctahedron, is sufficient to divide up the Pd fcc bulk without absence or overlap of the atoms. Furthermore, there is no such cluster which can be a unique constructing unit for the bcc lattice.

4.2.2. Enhancement of hydrogen adsorption. Hydrogen adsorption in Pd is known experimentally to be accelerated by its pre-adsorption. It appears as a horizontal part in the pressure–composition–temperature (PCT) plot for the Pd–H system [5]. As a typical example, at 473 K, hydrogen adsorption proceeds from the concentration $x = 0.075$ to $x = 0.46$ without increasing hydrogen pressure. In figure 9 we plot the total energy for $Pd_{13}H_n$, as a function of the number of the hydrogen atoms adsorbed at B′ or F sites. The energy change ΔE upon hydrogen adsorption is calculated from

$$\Delta E(Pd_{13}H_n) = E_{tot}(Pd_{13}H_n) - E_{tot}(Pd_{13}) - \frac{n}{2}E_{tot}(H_2)$$

where E_{tot} represents the total energy. The total energy for the adsorption at B′ sites and that at F sites are plotted separately, because these sites have different values of R_H and constituting electronic states of different CCS series. The decrement in E_{tot} caused by H adsorption increases as the adsorption proceeds up to six hydrogen atoms, i.e., hydrogen adsorption is accelerated. This is like a shell-closing effect. As a result of the adsorption of six hydrogen atoms at the same site (B′ or F) referred to the centre atom, the $1t_{1u}$ (1p) state of the CCS is occupied, resulting in shell closing of the 1p state (see section 3.2). Actually, the adsorption of the next two hydrogen atoms results in the additional occupation of the $1a_{2u}$ (1f) state, since the 1d state is already occupied by the Pd_c 4d electrons (figure 3(c)). The effect of the closing of $1t_{1u}$ on E_{tot} is large because there is almost no interaction between Pd_cH_8-$1t_{1u}$ and the peripheral Pd_{12}-$1t_{1u}$, while the interaction between Pd_cH_8-$1a_{2u}$ and peripheral Pd_{12}-$1a_{2u}$ is large; thus the effect of shell closing is smaller for $1a_{2u}$ (section 3.3). The enhancement in binding energy up to six hydrogen-atom adsorptions is also seen at the B site, but it is not seen for further H-atom adsorptions. The binding energy for $Pd_{13}H_6$ is larger than that for $Pd_{13}H_8$, where the adsorption occurs only at the B site. If R_H is important for this shell-closing effect, the six-atom occupation of the sites with the same R_H, e.g., B and B′ with $R_H = 3.4$ au, may cause the shell closing of the 1p state. This could be another driving force for the t-site occupation.

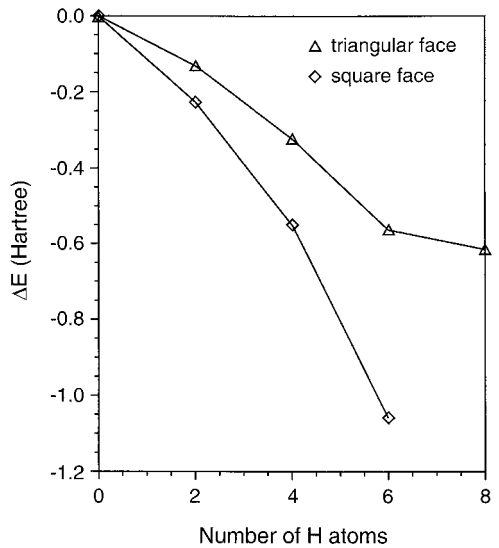

Figure 9. The change in the total energy versus the number (n) of adsorbed hydrogen atoms. Hydrogen adsorption takes place inside the square face (B′ site): ◇; or outside the triangular face (F site): △; respectively.

5. Summary

We have studied $Pd_{13}H_n$ clusters theoretically using the self-consistent density-functional scheme with a pseudopotential. We have mainly focused on Pd_{13}/H_n clusters.

Pseudo-spherically symmetric local minima appear in the total-energy plots of $Pd_{13}H_n$ clusters as functions of the distance of hydrogens from the cluster centre. Among these minima the most stable sites on the square and triangular faces of the cluster correspond to the o-sites in the fcc lattice. Two internal minima near the triangular face corresponding to the t-sites in the fcc lattice are considerably stabilized by the expanding Pd–Pd distance. Thus, $Pd_{13}H_n$ shows fundamental properties consistent with those derived from the experimental results for the bulk PdH system. According to the densities of states of $Pd_{13}H_n$ clusters and those of PdH crystal obtained by the LMTO band calculation, the former approximates the latter well, in particular when hydrogen atoms are adsorbed inside the cluster. The states induced by adsorbed hydrogen in the Pd_{13} cluster are explained by CCSs, which are formed by the bonding–anti-bonding interaction between the centre Pd_cH_n cluster and the peripheral Pd_{12} cluster. CCSs are located below the Pd d band and spatially localized near the cluster centre. The ability of the Pd_{13} cluster to store hydrogen is explained by the CCS vacancy around the H 1s energy and the lack of spherically symmetrical s and p states in the cluster-centre region. Since both CCSs and local minima in the total energy are caused by the spherically symmetrical nature, they are not seen in clusters smaller than the 13-atom cluster. Assuming $Pd_{13}H_8$ clusters with different hydrogen configurations for the α- and β-phases, we have calculated the change in the configuration entropy which may be attributable to the α-to-β transition in bulk $PdH_{0.6}$. The t-site occupation by hydrogen atoms is assumed to induce the α–β phase transition, as suggested by the expansion of the Pd–Pd distance in the $Pd_{13}H_n$ cluster ($n = 6, 8$) upon H adsorption at B sites.

Acknowledgments

One of the authors (NW) is indebted to Dr Tomi Ohtsuki of Sophia University, Dr Nobuyuki Nishimiya of the Toyohashi University of Technology, and Dr Norio Ookubo of NEC Functional Materials Research Laboratories for their valuable and encouraging support. She would like to thank Professor Kiyotaka Asakura of the University of Hokkaido and Dr Osamu Sugino of NEC Fundamental Research Laboratory for useful information on this work. We also wish to thank Takashi Ikeda of NEC Informatec Systems Limited, for producing the many three-dimensional figures used in this work.

References

[1] Graham T 1866 *Phil. Trans. R. Soc.* **156** 399
[2] Libowitz G G 1965 *The Solid State Chemistry of Binary Metal Hydrides* (New York: Benjamin)
[3] Lewis F A 1967 *The Pd–H System* (New York: Academic)
[4] Christmann K 1988 *Surf. Sci. Rep.* **9** 1
[5] Alefeld G and Völkl J 1978 *Hydrogen in Metals* vols 1 and 2 (Berlin: Springer)
[6] Bambakides G (ed) 1981 *Metal Hydrides (NATO Advanced Study Institute Series B, vol 76)* (New York: Plenum)
[7] Jena P and Satterthwaite C B (ed) 1983 *Electronic Structure and Properties of Hydrogen in Metals (NATO Conf. Series 6)* (New York: Plenum)
[8] Fukai Y and Sugimoto H 1985 *Adv. Phys.* **34** 263
[9] Ho K M, Elsässer C, Chan C T and Fähnle M 1992 *J. Phys.: Condens. Matter* **4** 5189
[10] Elsässer C, Ho K M, Chan C T and Fähnle M 1992 *J. Phys.: Condens. Matter* **4** 5207
[11] Elsässer C, Fähnle M and Schimmele L 1994 *Phys. Rev.* B **50** 5155
[12] Krimmel H, Schimmele L, Elsässer C and Fähnle M 1994 *J. Phys.: Condens. Matter* **6** 7679

[13] Katnel'son A A, Knyazeva M A, Revkevich G P and Olemskoi A L 1997 *Phys. Solid State* **39** 1132
[14] Switendick A C 1970 *Solid State Commun.* **8** 1463
Alefeld G and Völkl J 1978 *Hydrogen in Metals* vols 1 and 2 (Berlin: Springer) pp 101–29
[15] Papaconstantopoulos D A, Klein B M, Economou E N and Boyer L L 1978 *Phys. Rev.* B **17** 141
[16] Gupta M and Freeman A J 1978 *Phys. Rev.* B **17** 3029
[17] Jena P, Fradin F Y and Ellis D E 1979 *Phys. Rev.* B **20** 3543
[18] Chan C T and Louie S G 1983 *Phys. Rev.* B **27** 3325
[19] Watari N and Ohnishi S 1997 *J. Chem. Phys.* **106** 7531
[20] Ohnishi S and Watari N 1994 *Phys. Rev.* B **49** 14 619
[21] Perdew J P, Burke K and Ernzerhof M 1996 *Phys. Rev. Lett.* **77** 3865
[22] Watari N and Ohnishi S 1998 *Phys. Rev.* B **58** 1665
[23] Knight W D, Clemenger K, de Heer W A, Saunders W A, Chou M Y and Cohen M L 1984 *Phys. Rev. Lett.* **52** 2141
[24] Fukai Y 1993 *The Metal Hydrogen System* (Berlin: Springer)
[25] Fukai Y 1983 *Japan. J. Appl. Phys.* **22** 207
[26] Sugimoto H and Fukai Y 1980 *Phys. Rev.* B **22** 670
[27] Nordlander P, Nørskov J K and Besenbacher F 1986 *J. Phys. F: Met. Phys.* **16** 1161
[28] Ashman C, Khanna S N, Liu F, Kaplan T and Mostoller M 1997 *Phys. Rev.* B **55** 15 868
[29] Gong X G 1997 *Phys. Rev.* B **56** 1091